Nonlinear Dyn (2015) 79:835–849
DOI 10.1007/s11071-014-1706-5

ORIGINAL PAPER

Nonlinear vibration suppression of flexible structures using nonlinear modified positive position feedback approach

Ehsan Omidi · S. Nima Mahmoodi

Received: 28 February 2014 / Accepted: 9 September 2014 / Published online: 23 September 2014

Abstract This paper introduces Nonlinear Modified Positive Position Feedback (NMPPF) control approach for nonlinear vibration suppression at primary resonance. Nonlinearity in the system is due to large deformations caused by high-amplitude disturbances, while this control approach is applicable to all types of nonlinearities in resonant structures. NMPPF controller consists of a resonant second-order nonlinear compensator, which is enhanced by a lossy integrating compensator. The two compensators create a combination of exponential and periodic control inputs, which needs innovative time scaling for using the Method of Multiple Scales to obtain the analytical solution of the closed-loop system. The results of the analytical solution for the closed-loop NMPPF controller are presented and compared with the result of the conventional PPF controller. Effects of the control parameters on the system response are comprehensively studied by parameter variations. The approximate solution is then verified using numerical simulations. According to the results, the NMPPF controller provides a higher level of suppression in the overall frequency domain, as the peak amplitude at the neighborhood frequencies of the primary mode is reduced by 44 %, compared to the PPF method. The tunable control parameters also give more flexibility to create the expected type of system response.

Keywords Method of Multiple Scales · Nonlinear vibrations · Perturbation analysis · Positive Position Feedback · Vibration control

1 Introduction

Nonlinear vibrations occur in structures due to different causes, such as nonlinear properties of materials, geometric nonlinearities, and nonlinear external forces. In some cases, nonlinear terms can be neglected, but not when the system is under main resonance excitation with large motions [1,2]. Additionally, in micro-scale applications, nonlinearity of the system becomes more important as more accurate motion or measurement is required [3]. Resonant vibrations reduce system precision, as they may also damage the structure. As a solution to this problem, active vibration control techniques have been introduced and implemented [4]. Active vibration control is typically applied using piezoelectric ceramics as actuators and sensors, as these piezoelectric actuators have also been used in atomic force microscopes to produce high-frequency vibrations [5,6], forced vibrations of viscoelastic cantilevers [7], and precise motions [8,9].

E. Omidi · S. N. Mahmoodi (✉)
Nonlinear Intelligent Structures Laboratory, Department of Mechanical Engineering, The University of Alabama, Tuscaloosa, AL 35487-0276, USA
e-mail: nmahmoodi@eng.ua.edu

E. Omidi
e-mail: eomidi@crimson.ua.edu

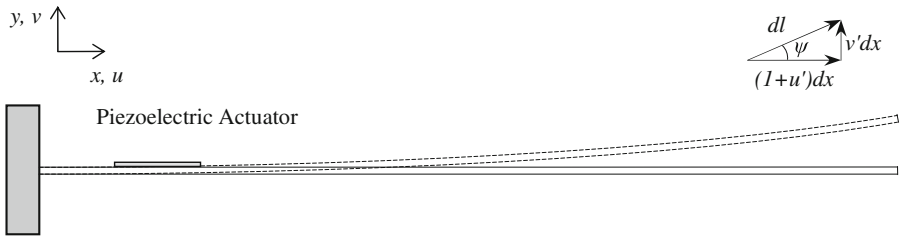

Fig. 1 The cantilever beam and the coordinates

Various types of controllers have been developed to channel the resonant excitation energy to a secondary system in order to attenuate vibrations in the main system. An example is the delayed-feedback approach, which has been used for nonlinear vibration control of a cantilever beam [10]. This control method focuses on the problem of intrinsic time delay between the control input and the real-time system actuation. Nonlinear saturation controller (NSC) is one of the frequently applied approaches [11], as it has been used with some other selected algorithms on a geometrically nonlinear beam-like composite structure [12,13]. Neural Network [14] and Receptance [15] are two other methods implemented for nonlinear vibration suppression. A control law based on cubic velocity feedback was proposed for a system under principal parametric excitation in single-mode control [16]. It has been discussed that the addition of a linear velocity feedback is mathematically equivalent to adding viscous damping and, therefore, would not be effective in reducing nonlinear vibrations. One of the methods that have been used for many vibration control purposes is the Positive Position Feedback (PPF) [17]. The PPF controller was later discussed and used for a nonlinear dynamic model [18,19]. Although unwanted vibrations are reduced to lower levels using the PPF controller, the closed-loop system becomes more flexible, leading to a larger steady-state error [20]. Therefore, a regular PPF controller may not necessarily provide the ultimate vibration attenuation level. To overcome this issue, a first-order compensator was added parallel to the second-order compensator. The results were the Modified Positive Position Feedback (MPPF) [21, 22], the Modified Positive Velocity Feedback (MPVF) [23], and the Modified Acceleration Feedback (MAF) [24].

In this paper, NMPPF approach is introduced and implemented for systems that undergo nonlinear vibrations. Here, large amplitude vibrations in the structure are the source of nonlinearity in the system. A cubic nonlinear term is added to the linear model of the MPPF controller to compensate for the cubic nonlinearities of the system model. The dynamic equation of the mechanical structure is obtained using the Hamilton principle [25]; then, the Method of Multiple Scales [26] is utilized to provide the closed-form solution for the closed-loop control system. The modulation equations are then used for the closed-loop stability and frequency response analyses. In the results section, performance of the new NMPPF and the conventional PPF approach are compared, and the influence of each parameter variation on the system response is demonstrated and discussed.

2 Mathematical modeling of the structure

A cantilever beam is considered as a flexible structure that undergoes large amplitude deflections. Figure 1 shows the schematic view of the beam and corresponding coordinates. u is the deformation in x direction, and v is the deformation in y axis. A piezoelectric ceramic is attached to the cantilever beam, to apply the required actuation moment to the beam. Since the thickness of the piezoelectric actuator is much smaller than the thickness of the beam, and it is attached just on a small length, the cantilever is assumed uniform.

According to Fig. 1, the bending angle ψ, is defined as:

$$\tan\psi = \frac{v'}{1+u'}, \tag{1}$$

where *prime* indicates the differentiation with respect to x. Strain e is then calculated such that [3,27]:

$$e = \frac{\mathrm{d}l}{\mathrm{d}x} - 1 = \frac{\sqrt{(1+u')^2+v'^2}\mathrm{d}x - \mathrm{d}x}{\mathrm{d}x} = \sqrt{(1+u')^2+v'^2} - 1. \tag{2}$$

where dl and dx are depicted in Fig. 1. Considering the assumption of inextensibility for the beam, the strain in the beam has to be equal to zero. Using Eq. (2) and the Taylor expansion, relationship between deformations is calculated as [6]:

$$u' = \sqrt{(1-v')^2} - 1 \approx -\frac{1}{2}v'^2. \tag{3}$$

The kinetic and potential energies are defined to be used in the Hamilton principle. The corresponding kinetic energy T and the potential energy U are expressed as [25]:

$$T = \frac{1}{2}\int_0^l m(\dot{u}^2 + \dot{v}^2)\mathrm{d}x, \text{ and} \tag{4}$$

$$U = \frac{1}{2}\int_0^l M_\mathrm{c}\frac{\partial \psi}{\partial x}\mathrm{d}x. \tag{5}$$

where the *over-dot* is the derivative with respect to t. M_c is the moment and for the considered structure is defined as [28]:

$$M_\mathrm{c} = -\int Eey\mathrm{d}A, \tag{6}$$

where E is the Young's Modulus of elasticity. Considering the bending angle of Eq. (1), curvature is calculated as [29]:

$$\rho = \frac{v''(1+u') - v'u''}{(1+u')^2 + v'^2}. \tag{7}$$

Using Eq. (7) and considering the uniformity of the beam's cross section, the moment is obtained. Substituting the moment into Eq. (5), and Eq. (3) into (4), the kinetic and potential energies become:

$$T = \frac{1}{2}\int_0^l m\left(\left[\frac{\partial}{\partial t}\int_0^x \frac{1}{2}v'^2\mathrm{d}x\right]^2 + \dot{v}^2\right)\mathrm{d}x, \text{ and} \tag{8}$$

$$U = \frac{1}{2}\int_0^l EI\left(v'' + \frac{1}{2}v''v'^2\right)^2\mathrm{d}x, \tag{9}$$

where I is the moment of inertia. Eqs. (8) and (9) are used in the Hamilton principle, considering F_v is the external force in the y direction. The resulting PDE and boundary conditions are:

$$m\ddot{v} + EIv^{iv} + \frac{m}{2}\left[v'\int_l^x\int_0^x(\dot{v}'^2 + v'\ddot{v}')\mathrm{d}x\mathrm{d}x\right]' + EI\left(v'(v'v'')'\right)' + F_v = 0, \tag{10}$$

$$v = v' = 0 \text{ at } x = 0, \text{ and } v'' = v''' = 0 \text{ at } x = l. \tag{11}$$

Note that in Eq. (10), $(.)^{iv}$ is the fourth derivative with respect to x.

3 NMPPF controller design

To obtain a closed-form solution for the PDE of Eq. (10), with the boundary conditions of (11), the Bubnov-Galerkin approximation method [30] is implemented. Separation of variables is performed such that $v(x,t) = \sum_{n=1}^{\infty}\phi_n(x)q_n(t)$, where $q_n(t)$ are the time-dependent variables and $\phi_n(t)$ are the linear mode shapes of the system, considered by the companion functions of:

$$\phi_n(x) = \cosh(\lambda_n x) - \cos(\lambda_n x) + \frac{\cosh(\lambda_n) + \cos(\lambda_n)}{\sin(\lambda_n) + \sinh(\lambda_n)} \times \left[\sin(\lambda_n x) - \sinh(\lambda_n x)\right], \tag{12}$$

where λ_n are the roots of the equation: $1 + \cos(\lambda_n)\cosh(\lambda_n) = 0$. Following the steps, resulting nonlinear ODE for fundamental mode of the cantilever beam becomes:

$$\ddot{q}(t) + \eta_q\dot{q}(t) + \omega_q^2 q(t) + \alpha q^3(t) + \beta q(t)\dot{q}^2(t) + \gamma q^2(t)\dot{q}(t) = F_r(t) + F_c(t). \tag{13}$$

In Eq. (13), $q(t)$ is the time-dependent variable of the system, and $F_c(t)$ is the control force. $F_r(t)$ is the resonant disturbance force substituted for F_v, and it is defined as: $F_r(t) = f\cos(\Omega t)$, where f is the amplitude and Ω is the frequency of the disturbance, respectively. $\eta_q = 2\mu_q\omega_q$, where μ_q is the damping ratio and ω_q is the frequency of the fundamental mode. α is the curvature nonlinearity coefficient, and β and γ are the inertia nonlinearity coefficients, which are defined as [31]:

$$\alpha = \frac{2\int_0^l EI\left[\phi_1''(x)\right]^2\left[\phi_1(x)\right]^2\mathrm{d}x}{\int_0^l m\left[\phi_1(x)\right]^2\mathrm{d}x}, \tag{14}$$

$$\beta = \gamma = \frac{2\int_0^l \phi_1(x)\left[m\phi_1'(x)\int_l^x\int_0^x 2\left[\phi_1'(x)\right]^2\mathrm{d}x\mathrm{d}x\right]'\mathrm{d}x}{\int_0^l m\left[\phi_1(x)\right]^2\mathrm{d}x}. \tag{15}$$

After having the system dynamics defined, the NMPPF controller is introduced. The NMPPF consists of two subsections of a second- and a first-order compensator. Since the nonlinearities of the system that are shown in Eq. (13) are cubic, a cubic nonlinear term is added to the second-order subsection. The first-order term which is basically a lossy integrator adds more damping to the structure, where the second-order term focuses on exact resonant frequency. The dynamic description of the NMPPF controller is described as:

$$\ddot{r}(t) + \eta_r \dot{r}(t) + \omega_r^2 r(t) + \delta r^3(t) = \kappa_r q(t), \tag{16}$$

$$\dot{s}(t) + \omega_s s(t) = \kappa_s q(t), \tag{17}$$

where $r(t)$ and $s(t)$ are state variables of the second- and first-order compensator, respectively. $\eta_r = 2\mu_r\omega_r$, where μ_r is the damping ratio and ω_r is the frequency of the secondary system. κ_r and κ_s are positive scalar constants, named as controller gains. In the PPF controller, the damping term of the compensator is considered high enough to suppress the resonant vibrations at the frequency of the compensator. In the MPPF, the frequency of the compensator (ω_r) is picked relatively close to the frequency of the system (ω_q), with very small damping factor of μ_r. The first-order term increases the damping of the closed-loop system, where ω_s may not necessarily be equal to ω_r. The control loop is closed by setting:

$$F_c(t) = \tau_r r(t) + \tau_s s(t), \tag{18}$$

where τ_r and τ_s are positive scalar feedback gains of second- and first-order compensators. Figure 2 shows the time-domain diagram representation of the closed-loop system.

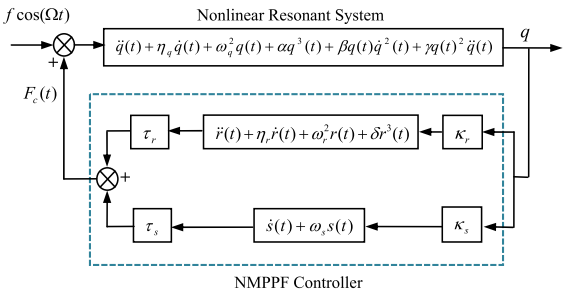

Fig. 2 Time-domain diagram of the NMPPF controlled system

4 Closed-loop system solution

Method of Multiple Scales is applied to find a uniform nonlinear approximate solution near the fundamental resonant mode of the structure [26]. To this end, two time scales of $T_0 = t$ and $T_1 = \varepsilon t$ are selected. Then, the time derivatives are defined as:

$$\frac{\mathrm{d}}{\mathrm{d}t} = D_0 + \varepsilon D_1 + \cdots, \tag{19}$$

$$\frac{\mathrm{d}^2}{\mathrm{d}t^2} = D_0^2 + 2\varepsilon D_0 D_1 + \cdots, \tag{20}$$

where $D_n = \partial/\partial T_n$ and ε is a bookkeeping parameter. Eqs. (19) and (20) are substituted in Eqs. (13), (16), and (17) that results in:

$$D_0^2 q + 2\varepsilon D_0 D_1 q + \eta_q D_0 q + \varepsilon\eta_q D_1 q + \omega_q^2 q + \alpha q^3 + \beta q \left(D_0 + \varepsilon D_1\right)^2 q^2 + \gamma q^2 \left(D_0 + \varepsilon D_1\right) q + \cdots = f\cos(\Omega t) + \tau_r r + \tau_s s, \tag{21}$$

$$D_0^2 r + 2\varepsilon D_0 D_1 r + \eta_r D_0 r + \varepsilon\eta_r D_1 r + \omega_r^2 r + \delta r^3 + \cdots = \kappa_r q, \tag{22}$$

$$D_0 s + \varepsilon D_1 s + \omega_s s + \cdots = \kappa_s q. \tag{23}$$

Parameters of the equations have to be scaled to appear in the same equations. Therefore, parameters are set as: $\eta_q = \varepsilon\hat{\eta}_q, \alpha = \varepsilon\hat{\alpha}, \beta = \varepsilon\hat{\beta}, \gamma = \varepsilon\hat{\gamma}, \tau_r = \varepsilon\hat{\tau}_r, \tau_s = \varepsilon\hat{\tau}_s, \eta_r = \varepsilon\hat{\eta}_r, \delta = \varepsilon\hat{\delta}, \kappa_r = \varepsilon\hat{\kappa}_r, \kappa_s = \hat{\kappa}_s$, and $f = \varepsilon\hat{f}$. Scaled parameters are substituted into the Eqs. (21)–(23); then, the variables $q(t)$, $r(t)$, and $s(t)$ are expanded by:

$$q(\varepsilon, T_0, T_1) = q_0(T_0, T_1) + \varepsilon q_1(T_0, T_1) + \cdots, \tag{24}$$

$$r(\varepsilon, T_0, T_1) = r_0(T_0, T_1) + \varepsilon r_1(T_0, T_1) + \cdots, \tag{25}$$

$$s(\varepsilon, T_0, T_1) = \varepsilon s_0(T_0, T_1) + \varepsilon^2 s_1(T_0, T_1) + \cdots. \tag{26}$$

where variables with 'zero' subscripts are the dominant solutions and subscripts of 'one' show small variations of the solutions. The order of Eq. (26) is selected higher than the other two equations and provides inhomogeneous scaling of the variables. The reason is to keep the first-order equation in pace with the other second-order equations. The result is separated in orders of ε, which yields to:

$\mathrm{O}(\varepsilon^0)$:

$$D_0^2 q_0 + \omega_q^2 q_0 = 0, \tag{27}$$

$$D_0^2 r_0 + \omega_r^2 r_0 = 0, \tag{28}$$

$O(\varepsilon^1)$:

$$D_0^2 q_1 + \omega_q^2 q_1 = \hat{f}\cos(\Omega T_0) + \hat{\tau}_r r_0 + \hat{\tau}_s s_0 - 2D_0 D_1 q_0 - \hat{\eta}_q D_0 q_0 - \hat{\alpha} q_0^3 - \hat{\beta} q_0 (D_0 q_0)^2 - \hat{\gamma} q_0^2 D_0 q_0, \quad (29)$$

$$D_0^2 r_1 + \omega_r^2 r_1 = \hat{\kappa}_r q_0 - \hat{\delta} r_0^3 - 2D_0 D_1 r_0 - \hat{\eta}_r D_0 r_0, \quad (30)$$

$$D_0 s_0 + \omega_s s_0 = \hat{\kappa}_s q_0, \quad (31)$$

$O(\varepsilon^2)$:

$$D_0 s_1 + \omega_s s_1 = \hat{\kappa}_s q_1 - D_1 s_0. \quad (32)$$

Order of ε^2 is considered just for the s, since it has a higher order of ε in the defined expansion of (26). This is required to have the solution for s_1. The solution to the homogeneous differential equations of (27) and (28) could be expressed as:

$$q_0 = A(T_1)e^{i\omega_q T_0} + \bar{A}(T_1)e^{-i\omega_q T_0}, \quad (33)$$

$$r_0 = B(T_1)e^{i\omega_r T_0} + \bar{B}(T_1)e^{-i\omega_r T_0}, \quad (34)$$

where $A(T_1)$ and $B(T_1)$ are complex-valued functions that will be determined by eliminating the secular and small-divisor terms at a later stage of the analysis, and the *over-bar* is the complex conjugate function. Eq. (33) is substituted into (31), and the ODE is solved. The result is:

$$s_0 = C(T_1)e^{-\omega_s T_0} + \frac{\hat{\kappa}_s}{\omega_q^2 + \omega_s^2}\left(\omega_s - i\omega_q\right)A(T_1)e^{i\omega_q T_0} + \frac{\hat{\kappa}_s}{\omega_q^2 + \omega_s^2}\left(\omega_s + i\omega_q\right)\bar{A}(T_1)e^{-i\omega_q T_0}, \quad (35)$$

where $C(T_1)$ is going to be obtained in further steps of the solution. Next, Eqs. (33)–(35) are substituted into the Eqs. (29)–(30). The simplified result is:

$$\begin{aligned} D_0^2 q_1 + \omega_q^2 q_1 &= \frac{\hat{f}}{2}e^{i\Omega T_0} + \hat{\tau}_r\left(B(T_1)e^{i\omega_r T_0} + \bar{B}(T_1)e^{-i\omega_r T_0}\right) \\ &+\hat{\tau}_s\left(C(T_1)e^{-\omega_s T_0} + \frac{\hat{\kappa}_s}{\omega_q^2+\omega_s^2}\left(\omega_s - i\omega_q\right)A(T_1)e^{i\omega_q T_0} + \frac{\hat{\kappa}_s}{\omega_q^2+\omega_s^2}\left(\omega_s + i\omega_q\right)\bar{A}(T_1)e^{-i\omega_q T_0}\right) \\ &-\Big[\left(\hat{\eta}_q A(T_1) + 2D_1 A(T_1)\right) i\omega_q e^{i\omega_q T_0} \\ &-\left(\hat{\eta}_q \bar{A}(T_1) + 2D_1 \bar{A}(T_1)\right) i\omega_q e^{-i\omega_q T_0}\Big] \\ &-\hat{\alpha}\left(A(T_1)e^{i\omega_q T_0} + \bar{A}(T_1)e^{-i\omega_q T_0}\right)^3 \\ &+\hat{\beta}\omega_q^2\left(A(T_1)e^{i\omega_q T_0} + \bar{A}(T_1)e^{-i\omega_q T_0}\right) \\ &\left(A(T_1)e^{i\omega_q T_0} - \bar{A}(T_1)e^{-i\omega_q T_0}\right)^2 \\ &-\hat{\gamma}\omega_q i\left(A(T_1)e^{i\omega_q T_0} + \bar{A}(T_1)e^{-i\omega_q T_0}\right)^2 \\ &\left(A(T_1)e^{i\omega_q T_0} - \bar{A}(T_1)e^{-i\omega_q T_0}\right), \end{aligned} \quad (36)$$

$$\begin{aligned} D_0^2 r_1 + \omega_r^2 r_1 &= \hat{\kappa}_r\left(A(T_1)e^{i\omega_q T_0} + \bar{A}(T_1)e^{-i\omega_q T_0}\right) \\ &-\Big[\left(\hat{\eta}_r B(T_1) + 2D_1 B(T_1)\right) i\omega_r e^{i\omega_r T_0} \\ &-\left(\hat{\eta}_r \bar{B}(T_1) + 2D_1 \bar{B}(T_1)\right) i\omega_r e^{-i\omega_r T_0}\Big] \\ &-\hat{\delta}\left(B(T_1)e^{i\omega_r T_0} + \bar{B}(T_1)e^{-i\omega_r T_0}\right)^3. \end{aligned} \quad (37)$$

q_1 and r_1 are calculated using Eqs. (36) and (37) in time domain such that:

$$q_1 = Q_1 e^{i\Omega T_0} + Q_2 e^{i\omega_r T_0} + Q_3 e^{-\omega_s T_0} + Q_4 e^{3i\omega_q T_0} + cc, \quad (38)$$

where

$$Q_1 = \frac{\hat{f}/2}{\omega_q^2 - \Omega^2}, \quad Q_2 = \frac{\hat{\tau}_r B(T_1)}{\omega_q^2 - \omega_r^2}, \quad Q_3 = \frac{\hat{\tau}_s C(T_1)}{\omega_q^2 + \omega_s^2},$$

and $Q_4 = -\dfrac{\left[i\hat{\gamma}\omega_s + \hat{\alpha} - \hat{\beta}\omega_q^2\right]A^3(T_1)}{8\omega_q^2}$.

$$r_1 = R_1 e^{i\omega_q T_0} + R_2 e^{3i\omega_r T_0} + cc, \quad (39)$$

where

$$R_1 = \frac{\hat{\kappa}_r A(T_1)}{\omega_r^2 - \omega_q^2}, \text{ and } R_2 = \frac{\hat{\delta}B^3(T_1)}{8\omega_r^2}.$$

In order to solve for s_1, Eqs. (35) and (38) are substituted into (32) to form the ODE of:

$$\begin{aligned} D_0 s_1 + \omega_s s_1 &= \hat{\kappa}_s Q_1 e^{i\Omega T_0} + \hat{\kappa}_s Q_2 e^{i\omega_r T_0} \\ &+\left(\hat{\kappa}_s Q_3 - D_1 C(T_1)\right)e^{-\omega_s T_0} \\ &+\hat{\kappa}_s Q_4 e^{3i\omega_q T_0} - \frac{\hat{\kappa}_s}{\omega_q^2 + \omega_s^2} \\ &\times\left(\omega_s - i\omega_q\right)D_1 A(T_1)e^{i\omega_q T_0} + cc, \end{aligned} \quad (40)$$

where cc is the complex conjugate of terms. The solution to the ODE of Eq. (40) is:

$$s_1 = S_1 e^{i\Omega T_0} + S_2 e^{i\omega_r T_0} + S_3 e^{3i\omega_q T_0} + S_4 e^{i\omega_q T_0} + cc, \tag{41}$$

where

$$S_1 = \frac{\hat{\kappa}_s Q_1}{\omega_s^2 + \Omega^2}\left(\omega_s - i\Omega\right),$$

$$S_2 = \frac{\hat{\kappa}_s Q_2}{\omega_s^2 + \omega_r^2}\left(\omega_s - i\omega_r\right),$$

$$S_3 = \frac{\hat{\kappa}_s Q_4}{\omega_s^2 + 9\omega_q^2}\left(\omega_s - 3i\omega_q\right), \text{ and}$$

$$S_4 = \frac{\hat{\kappa}_s D_1 A(T_1)}{\left(\omega_q^2 + \omega_s^2\right)^2}\left(\omega_q^2 - \omega_s^2 + 2i\omega_s\omega_q\right).$$

For the system to have a bounded solution, summation of the secular terms has to be equal to zero. Applying this condition to Eq. (40), $C(T_1)$ is calculated as:

$$C(T_1) = c_s e^{\left(\frac{\hat{\kappa}_s\hat{\tau}_s}{\omega_q^2+\omega_s^2}\right)T_1}, \tag{42}$$

where c_s is a constant. Next step is to sort Eqs. (36) and (37) and separate the secular terms as:

$$\begin{aligned} &D_0^2 q_1 + \omega_q^2 q_1 \\ &= \frac{\hat{f}}{2}e^{i\Omega T_0} + \hat{\tau}_r B(T_1)e^{i\omega_r T_0} + \hat{\tau}_s C(T_1)e^{-\omega_s T_0} \\ &\quad - \left[i\hat{\gamma}\omega_q + \hat{\alpha} - \hat{\beta}\omega_q^2\right]A^3(T_1)e^{3i\omega_q T_0} \\ &\quad - \left[\left(\hat{\eta}_q A(T_1) + 2D_1 A(T_1)\right)i\omega_q\right. \\ &\quad + A^2(T_1)\bar{A}(T_1)\left(3\hat{\alpha} + \hat{\beta}\omega_q^2 + i\hat{\gamma}\omega_q\right) \\ &\quad \left. + \frac{\hat{\tau}_s\hat{\kappa}_s}{\omega_q^2+\omega_s^2}A(T_1)\left(\omega_s - i\omega_q\right)\right]e^{i\omega_q T_0} \\ &\quad + cc, \end{aligned} \tag{43}$$

$$\begin{aligned} &D_0^2 r_1 + \omega_r^2 r_1 = \hat{\kappa}_r A(T_1)e^{i\omega_q T_0} - \hat{\delta}B^3(T_1)e^{3i\omega_r T_0} \\ &\quad - \left(\hat{\eta}_r B(T_1) + 2D_1 B(T_1) - 3i\hat{\delta}B^2(T_1)\bar{B}(T_1)\right) \\ &\quad \times i\omega_r e^{i\omega_r T_0} + cc. \end{aligned} \tag{44}$$

Since the frequencies of the second-order compensator, disturbance excitation, and main system are very close to each other, the detuning parameters of σ_r and σ_f are defined. Using the small scale detuning parameters, the frequencies are redefined as:

$$\begin{cases} \omega_r = \omega_q + \varepsilon\sigma_r, \\ \Omega = \omega_q + \varepsilon\sigma_f, \end{cases} \tag{45}$$

Eliminating the secular terms in Eqs. (43) and (44) yields to:

$$\begin{bmatrix} \frac{\hat{f}}{2}e^{i\sigma_f T_1} + \hat{\tau}_r B(T_1)e^{i\sigma_r T_1} \\ \quad + \frac{\hat{\tau}_s\hat{\kappa}_s}{\omega_q^2+\omega_s^2}\left(\omega_s - i\omega_q\right)A(T_1) \\ \quad - \left(\hat{\eta}_q A(T_1) + 2D_1 A(T_1)\right)i\omega_q \\ \quad - A^2(T_1)\bar{A}(T_1)\left(3\hat{\alpha} + \hat{\beta}\omega_q^2 + i\hat{\gamma}\omega_q\right) \end{bmatrix} e^{i\omega_q T_0} = 0, \tag{46}$$

$$\begin{bmatrix} \hat{\kappa}_r A(T_1)e^{-i\sigma_r T_1} - 3\hat{\delta}B^2(T_1)\bar{B}(T_1) \\ \quad - \left(\hat{\eta}_r B(T_1) + 2D_1 B(T_1)\right)i\omega_r \end{bmatrix} e^{i\omega_r T_0} = 0. \tag{47}$$

To solve Eqs. (46) and (47), it is convenient to express the solution in polar form:

$$A(T_1) = \frac{1}{2}a(T_1)e^{i\zeta_a(T_1)}, \tag{48}$$

$$B(T_1) = \frac{1}{2}b(T_1)e^{i\zeta_b(T_1)}. \tag{49}$$

Equations (48) and (49) are substituted into (46) and (47); then, real and imaginary parts are separated, and amplitude-phase modulating equations are extracted as:

$$\begin{aligned} D_1 a(T_1) &= -\frac{\hat{\eta}_q}{2}a(T_1) - \frac{\hat{\tau}_s\hat{\kappa}_s}{\omega_q^2+\omega_s^2}a(T_1) \\ &\quad + \frac{\hat{f}}{2\omega_q}\sin(\sigma_f T_1 - \zeta_a(T_1)) \\ &\quad + \frac{\hat{\tau}_r}{2\omega_q}b(T_1)\sin(\sigma_r T_1 + \zeta_b(T_1) - \zeta_a(T_1)) \\ &\quad + \frac{\hat{\gamma}}{8}a^3(T_1), \end{aligned} \tag{50}$$

$$\begin{aligned} D_1\zeta_a(T_1) &= \frac{1}{8\omega_q}a^2(T_1)\left(3\hat{\alpha} + \hat{\beta}\omega_q^2\right) - \frac{\hat{\tau}_s\hat{\kappa}_s\omega_s}{(\omega_q^2+\omega_s^2)\omega_q} \\ &\quad - \frac{\hat{f}}{2\omega_q a(T_1)}\cos(\sigma_f T_1 - \zeta_a(T_1)) \\ &\quad - \frac{\hat{\tau}_r b(T_1)}{2\omega_q a(T_1)}\cos(\sigma_r T_1 + \zeta_b(T_1) - \zeta_a(T_1)), \end{aligned} \tag{51}$$

$$\begin{aligned} D_1 b(T_1) &= -\frac{\hat{\eta}_r}{2}b(T_1) + \frac{\hat{\kappa}_r}{2\omega_r}a(T_1)\sin(\zeta_a(T_1) \\ &\quad - \sigma_r T_1 - \zeta_b(T_1)), \end{aligned} \tag{52}$$

$$\begin{aligned} D_1\zeta_b(T_1) &= \frac{3\hat{\delta}}{8\omega_r}b^2(T_1) - \frac{\hat{\kappa}_r a(T_1)}{2\omega_r b(T_1)}\cos(\zeta_a(T_1) \\ &\quad - \sigma_r T_1 - \zeta_b(T_1)). \end{aligned} \tag{53}$$

Since all variables of Eqs. (50)–(53) are functions of T_1, equations could be transformed to the t-domain.

In order to obtain the autonomous equation set, it is considered that $\theta_a(t) = \sigma_f t - \zeta_a(t)$ and $\theta_b(t) = \sigma_r t + \zeta_b(t) - \zeta_a(t)$. Using the transformation, the modulation equations are expressed as:

$$\dot{a} = -\left(\frac{\hat{\eta}_q}{2} + \frac{\hat{\tau}_s\hat{\kappa}_s}{\omega_q^2+\omega_s^2}\right)a + \frac{\hat{f}}{2\omega_q}\sin(\theta_a) + \frac{\hat{\tau}_r}{2\omega_q}b\sin(\theta_b) + \frac{\hat{\gamma}}{8}a^3, \tag{54}$$

$$\dot{\theta}_a = -\frac{1}{8\omega_q}\left(3\hat{\alpha}+\hat{\beta}\omega_q^2\right)a^2 + \frac{\hat{\tau}_s\hat{\kappa}_s\omega_s}{(\omega_q^2+\omega_s^2)\omega_q} + \frac{\hat{f}}{2\omega_q}\frac{1}{a}\cos(\theta_a) + \frac{\hat{\tau}_r}{2\omega_q}\frac{b}{a}\cos(\theta_b) + \sigma_f, \tag{55}$$

$$\dot{b} = -\frac{\hat{\eta}_r}{2}b - \frac{\hat{\kappa}_r}{2\omega_r}a\sin(\theta_b), \tag{56}$$

$$\dot{\theta}_b = \frac{3\hat{\delta}}{8\omega_r}b^2 + \frac{\hat{f}}{2\omega_q}\frac{1}{a}\cos(\theta_a) + \left(\frac{\hat{\tau}_r b}{2\omega_q a} - \frac{\hat{\kappa}_r a}{2\omega_r b}\right)\cos(\theta_b) - \frac{1}{8\omega_q}\left(3\hat{\alpha}+\hat{\beta}\omega_q^2\right)a^2 + \frac{\hat{\tau}_s\hat{\kappa}_s\omega_s}{(\omega_q^2+\omega_s^2)\omega_q} + \sigma_r. \tag{57}$$

5 Frequency response and stability analysis

In this section, frequency response of the system will be extracted. The steady-state condition of the closed-loop system is considered by setting:

$$\dot{a} = \dot{\theta}_a = 0, \text{ and } \dot{b} = \dot{\theta}_b = 0. \tag{58}$$

Applying the conditions of (58) to Eqs. (54)–(57) yields to:

$$\frac{\hat{f}}{2\omega_q}\sin(\theta_a) = \left(\frac{\hat{\eta}_q}{2} + \frac{\hat{\tau}_s\hat{\kappa}_s}{\omega_q^2+\omega_s^2}\right)a + \frac{\hat{\tau}_r\omega_r\hat{\eta}_r}{2\omega_q\hat{\kappa}_r}\frac{b^2}{a} - \frac{\hat{\gamma}}{8}a^3, \tag{59}$$

$$\frac{\hat{f}}{2\omega_q}\cos(\theta_a) = \frac{1}{8\omega_q}\left(3\hat{\alpha}+\hat{\beta}\omega_q^2\right)a^3 - \frac{\hat{\tau}_s\hat{\kappa}_s\omega_s}{(\omega_q^2+\omega_s^2)\omega_q}a - \frac{3\hat{\delta}\hat{\tau}_r}{8\omega_q\hat{\kappa}_r}\frac{b^4}{a} - \frac{\hat{\tau}_r\omega_r}{\hat{\kappa}_r\omega_q}\left(\sigma_r-\sigma_f\right)\frac{b^2}{a} - \sigma_f a, \tag{60}$$

$$\sin(\theta_b) = -\frac{\omega_r\hat{\eta}_r}{\hat{\kappa}_r}\frac{b}{a}, \text{ and} \tag{61}$$

$$\cos(\theta_b) = \frac{3\hat{\delta}}{4\hat{\kappa}_r}\frac{b^3}{a} + \frac{2\omega_r}{\hat{\kappa}_r}\left(\sigma_r-\sigma_f\right)\frac{b}{a}. \tag{62}$$

Using Eqs. (59)–(62), the frequency response is obtained in terms of two coupled equations as:

$$\frac{\hat{f}^2}{4\omega_q^2} = \left[\left(\frac{\hat{\eta}_q}{2} + \frac{\hat{\tau}_s\hat{\kappa}_s}{\omega_q^2+\omega_s^2}\right)a + \frac{\hat{\tau}_r\omega_r\hat{\eta}_r}{2\omega_q\hat{\kappa}_r}\frac{b^2}{a} - \frac{\hat{\gamma}}{8}a^3\right]^2 + \left[\frac{1}{8\omega_q}\left(3\hat{\alpha}+\hat{\beta}\omega_q^2\right)a^3 - \frac{\hat{\tau}_s\hat{\kappa}_s\omega_s}{(\omega_q^2+\omega_s^2)\omega_q}a - \frac{3\hat{\delta}\hat{\tau}_r}{8\hat{\kappa}\omega_q}\frac{b^4}{a} - \frac{\hat{\tau}_r\omega_r}{\hat{\kappa}_r\omega_q}\left(\sigma_r-\sigma_f\right)\frac{b^2}{a} - \sigma_f a\right]^2, \tag{63}$$

$$\left[1 - \frac{\omega_r^2\hat{\eta}_r^2}{\hat{\kappa}_r^2}\frac{b^2}{a^2}\right]^{\frac{1}{2}} = \frac{2\omega_r}{\hat{\kappa}_r}\left(\sigma_r-\sigma_f\right)\frac{b}{a} + \frac{3\hat{\delta}}{4\hat{\kappa}_r}\frac{b^3}{a}, \tag{64}$$

where Eqs. (63) and (64) are used to solve the frequency-domain amplitudes of the main system and the second-order compensator. Stability properties of the solution are examined around the equilibrium point expressed in Eq. (58). To this end, the Jacobian matrix of the equation set of (54)–(57) using Eqs. (59)–(62) is calculated by considering the variable set of:

$$\mathrm{X} = \left[a\ \theta_a\ b\ \theta_b\right]. \tag{65}$$

The Jacobian matrix $\bar{J}$ is given by:

$$\bar{J} = \begin{bmatrix} J_{11} & J_{12} & J_{13} & J_{14} \\ J_{21} & J_{22} & J_{23} & J_{24} \\ J_{31} & J_{32} & J_{33} & J_{34} \\ J_{41} & J_{42} & J_{43} & J_{44} \end{bmatrix}, \tag{66}$$

where

$$J_{11} = -\left(\frac{\hat{\eta}_q}{2} + \frac{\hat{\tau}_s\hat{\kappa}_s}{\omega_q^2+\omega_s^2}\right) + \frac{\hat{\gamma}}{8}a^3,$$

$$J_{12} = \frac{1}{8\omega_q}\left(3\hat{\alpha}+\hat{\beta}\omega_q^2\right)a^3 - \frac{\hat{\tau}_s\hat{\kappa}_s\omega_s}{(\omega_q^2+\omega_s^2)\omega_q}a - \frac{3\hat{\delta}\hat{\tau}_r}{8\omega_q\hat{\kappa}_r}\frac{b^4}{a} - \frac{\hat{\tau}_r\omega_r}{\hat{\kappa}_r\omega_q}\left(\sigma_r-\sigma_f\right)\frac{b^2}{a} - \sigma_f a,$$

$$J_{13} = -\frac{\omega_r\hat{\eta}_r\hat{\tau}_r}{2\omega_q\hat{\kappa}_r}\frac{1}{a},$$

$$J_{14} = \frac{3\hat{\tau}_r\hat{\delta}}{8\omega_q\hat{\kappa}_r}\frac{b^3}{a} + \frac{\hat{\tau}_r\omega_r}{\hat{\kappa}_r\omega_q}\left(\sigma_r-\sigma_f\right)\frac{b}{a},$$

$$J_{21} = -\frac{9}{8}\omega_q\left(\hat{\beta}+\hat{\gamma}+\hat{\alpha}/\omega_q^2\right)a + \frac{\hat{\tau}_s\hat{\kappa}_s\omega_s}{(\omega_q^2+\omega_s^2)\omega_q}\frac{1}{a} + \frac{\sigma_f}{a},$$

$$J_{22} = -\left(\frac{\eta_q}{2} + \frac{\hat{\tau}_s \hat{\kappa}_s}{\omega_q^2 + \omega_s^2}\right) - \frac{\hat{\tau}_r \omega_r \hat{\eta}_r}{2\omega_q \hat{\kappa}_r} \frac{b^2}{a^2},$$

$$J_{23} = \frac{3\hat{\tau}_r \hat{\delta}}{8\omega_q \hat{\kappa}_r} \frac{b^3}{a^2} + \frac{\hat{\tau}_r \omega_r}{\hat{\kappa}_r \omega_q} \left(\sigma_r - \sigma_f\right) \frac{b}{a^2},$$

$$J_{24} = \frac{\hat{\tau}_r \hat{\eta}_r \omega_r}{\hat{\kappa}_r \omega_q} \frac{b^2}{a^2},$$

$$J_{31} = \frac{\hat{\eta}_r}{2} \frac{b}{a}, J_{32} = 0, J_{33} = -\frac{\hat{\eta}_r}{2},$$

$$J_{34} = \left(\sigma_f - \sigma_r\right) b - \frac{3\hat{\delta}}{8\omega_r} b^3,$$

$$J_{41} = J_{21} - \frac{3\hat{\delta}}{8\omega_r} \frac{b^2}{a} + \left(\sigma_f - \sigma_r\right) \frac{1}{a},$$

$$J_{42} = J_{22},$$

$$J_{43} = \frac{3\hat{\delta}}{4\omega_r} b + \left(\frac{\hat{\tau}_r}{2\omega_q} \frac{1}{a} + \frac{\hat{\kappa}_r}{2\omega_r} \frac{a}{b^2}\right) \times \left(\frac{3\delta}{4\hat{\kappa}_r} \frac{b^3}{a} + \frac{2\omega_r}{\hat{\kappa}_r} \left(\sigma_r - \sigma_f\right) \frac{b}{a}\right), \quad J_{44} = 0.$$

Having the arrays of the Jacobian matrix calculated, the characteristic equation of the matrix is calculated by:

$$\det\left(\bar{J} - \hat{\lambda} I\right) = 0. \tag{67}$$

Equation (67) provides the eigenvalue equation as:

$$a_0 \hat{\lambda}^4 + a_1 \hat{\lambda}^3 + a_2 \hat{\lambda}^2 + a_3 \hat{\lambda} + a_4 = 0, \tag{68}$$

where values for $\hat{\lambda}$ are eigenvalues of the Jacobian matrix and a_i are coefficients of the characteristic equation. The stability of the equilibrium state is determined by the signs of the real parts of the eigenvalues of the characteristic equation. The *Routh-Hurwitz* stability criterion demands that for a stable system the real parts of all of eigenvalues should be negative [32]. Based on this criterion to have the system stable, the necessary and sufficient conditions are:

$$a_i > 0 \ (i = 0, \ldots, 4), a_1 a_2 - a_0 a_3 > 0,$$
$$a_1 a_2 a_3 - a_0 a_3^2 - a_1 a_4^2 > 0 \tag{69}$$

6 Results and discussions

In this section, the frequency response of the system is presented, and then, a comparison between performances of the NMPPF and the PPF controller is presented to investigate and compare the efficiency of the new approach. Then, the frequency response of the closed-loop system is studied in more detail by analyzing the sensitivity of fundamental parameters of the control system.

6.1 Frequency response of the nonlinear resonant system

Before studying the closed-loop system, it is necessary to present an illustration of the uncontrolled system response. The open-loop solution of the system is obtained using Eqs. (63) and (64). Numerical values of the main system are listed in Table 1. Figure 3 shows the frequency response of the uncontrolled system. The dashed line shows the unstable region in the frequency graph. The system behaves linearly for low amplitude excitations (e.g., for $f = 0.02$). Vibration amplitudes do not exceed the allowable limit, which is assigned linear systems. The *jump phenomenon* is observed in higher amplitude excitations.

Table 1 Numerical values of the main system

Variable	ω_q	μ_q	α	β, γ
Value	4.5	0.015	18.5	4

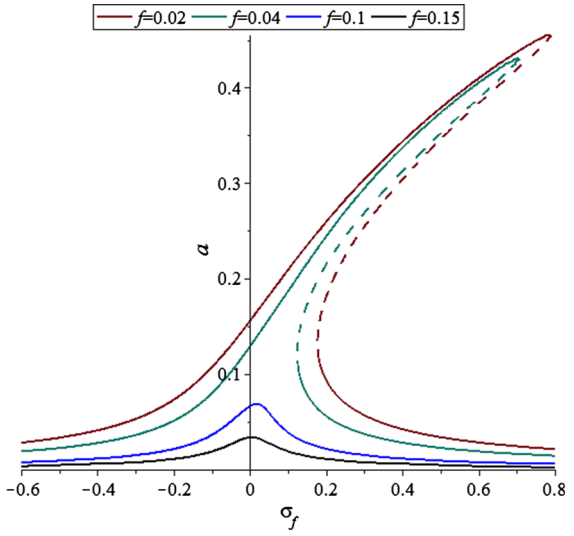

Fig. 3 Frequency response of the flexible structure under different excitation amplitudes

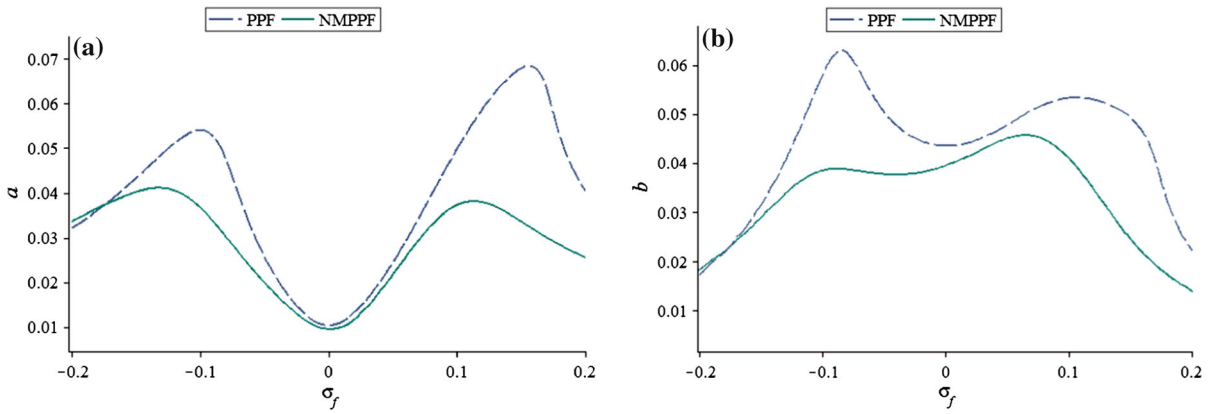

Fig. 4 Frequency response of the controlled systems using PPF and NMPPF approaches. **a** The resonant system, **b** the resonant controller

6.2 PPF and NMPPF controllers comparison

In this section, closed-loop solutions of the NMPPF and the well-known PPF approach controlled systems are examined and compared. Numerical values of the gains and controller parameters of the PPF controller are matched with the values of the NMPPF controller, where $\omega_r = \omega_s = 4.5, \mu_r = 0.006, \delta = 10, \kappa_r = \tau_r = 1, \kappa_s = \tau_s = 1.4$. Figure 4a shows the closed-loop frequency responses of the PPF and NMPPF controllers for the excitation amplitude of $f = 0.06$. According to the controlled result and considering the uncontrolled state in Fig. 3, the PPF controller has suitable suppression on the vibration amplitude at exact resonance value ($\sigma_f = 0$). However, as the excitation frequency deviates from the origin, two peaks occur at $\sigma_f = -0.12$ and $\sigma_f = 0.26$ with relatively large amplitudes. The NMPPF controller has slightly better suppression at exact resonance compared to the PPF. In addition, the amplitude of the maximum peak in the NMPPF controlled system response is 44 % lower than the maximum amplitude of the PPF controlled system. Figure 4b shows the resonant controller's amplitude using the two approaches. Resonant controller amplitude is also lower using the NMPPF controller as a result of the lower amplitude in the corresponding main system response. In Ref. [12], performance of the PPF controller has been compared to three other feedback controllers with a simple gain, cubic displacement, and nonlinear saturation control method. According to the results in the mentioned reference, the PPF controller has a higher level of suppression in comparison with the other controllers. Considering this fact and the obtained result in Fig. 4, the superiority of the NMPPF controller to the other approaches is also justified.

Table 2 Numerical values of the NMPPF controller

Variable	Value	Variable	Value
ω_r	4.5	κ_r	2
μ_r	0.002	κ_s	2
ω_s	4.5	τ_r	1
δ	0	τ_s	1

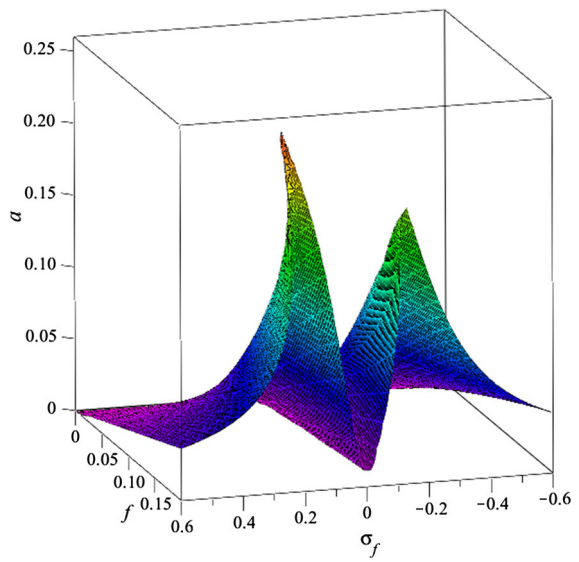

Fig. 5 Resonant system amplitude under NMPPF controller versus excitation amplitude and frequency

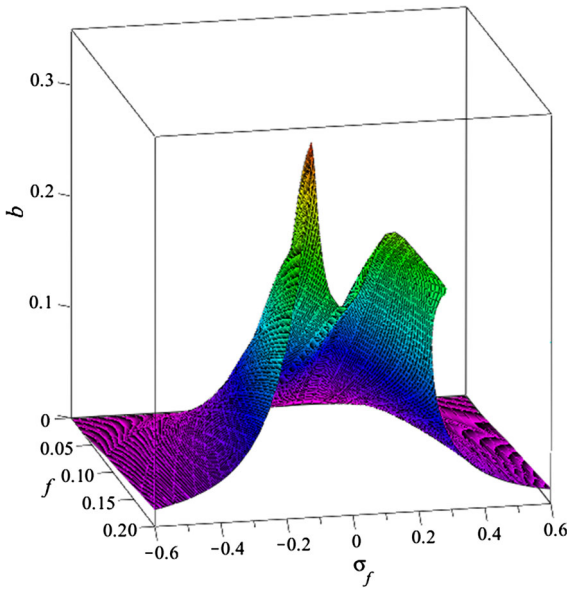

Fig. 6 NMPPF compensator amplitude versus excitation amplitude and frequency

6.3 NMPPF controller analysis

Performance of the NMPPF controller is discussed in more detail here. Different parameters are varied, and response of the system under the changes is investigated. Table 2 shows the default numerical values that are selected for the system analysis. The closed-loop system response is a function of the excitation amplitude as well as the excitation frequency. Hence, Figs. 5 and 6 show the response of the system and compensator's amplitude to excitation amplitude and frequency. For lower values of excitation amplitude, *jump phenomenon* is not observed in the response. As the excitation amplitude increases and passes the margin of $f = 0.13$, the nonlinear jump occurs in the frequency response of the main system. The peak at the negative side of the σ_f axis experiences the frequency shift, but does not undergo the amplitude jump. Compensator amplitude peak value on the negative side of the σ_f axis is much larger than the other peak in the positive side. The jump at the compensator frequency response amplitude occurs for values of excitation amplitude above $f = 0.17$, and it also happens at the positive side peak.

The first parameter to consider is μ_r. Figure 7 shows the amplitudes of the main system and controller under different values of μ_r. The excitation amplitude for the rest of the analyses is considered as $f = 0.04$. According to Fig. 7a, increments in μ_r result in a higher-level suppression of the resonant system in the overall bandwidth of excitation. However, as μ_r increases, suppression at exact point of resonance decreases.

The other parameter that has a very significant effect on the suppression performance is the second-order compensator's frequency. The effect of variation of this parameter is studied by changes in the corresponding detuning parameter, σ_r. However, since the controller performance is dependent on the excitation frequency too, vibration amplitude is depicted as a function of both frequencies in Fig. 8. The most important result of this graph is that the highest level of suppression happens for the line $\sigma_r = \sigma_f$. In other words, in order

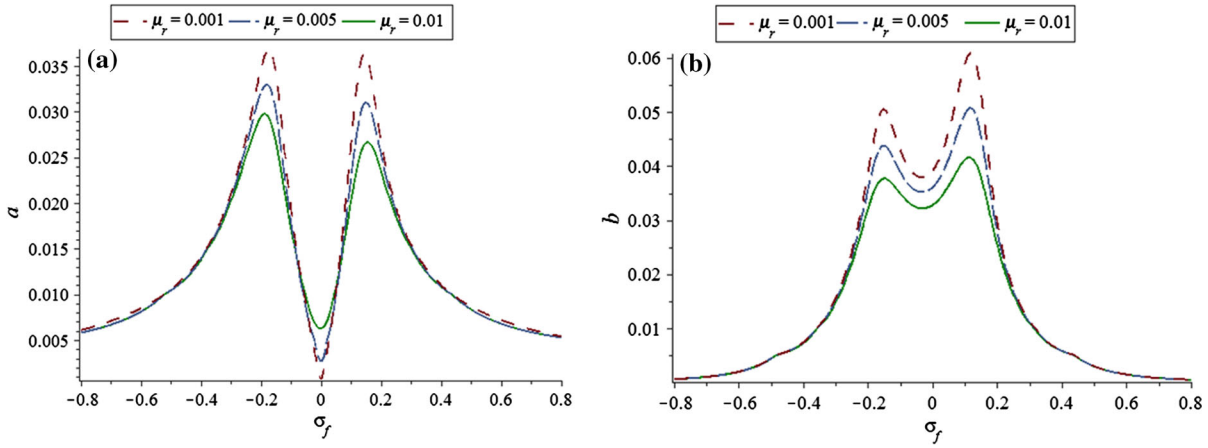

Fig. 7 Frequency response of the closed-loop system for values of μ_r, **a** the resonant system, **b** the resonant controller

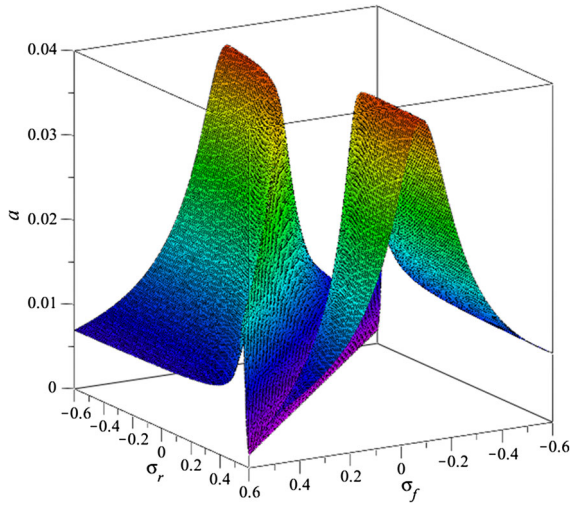

Fig. 8 Resonant system amplitude under NMPPF controller versus excitation and compensation frequencies

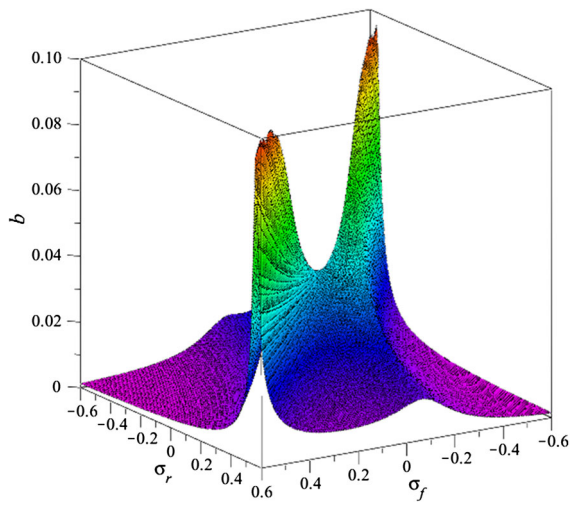

Fig. 9 NMPPF compensator amplitude versus excitation and compensation frequencies

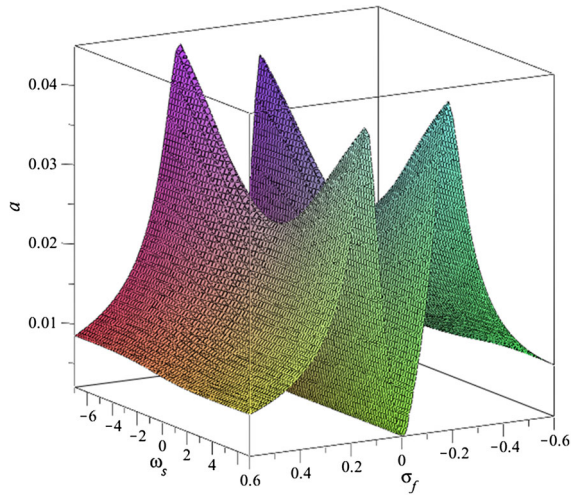

Fig. 10 Resonant system amplitude under NMPPF controller versus excitation and lossy integrator frequencies

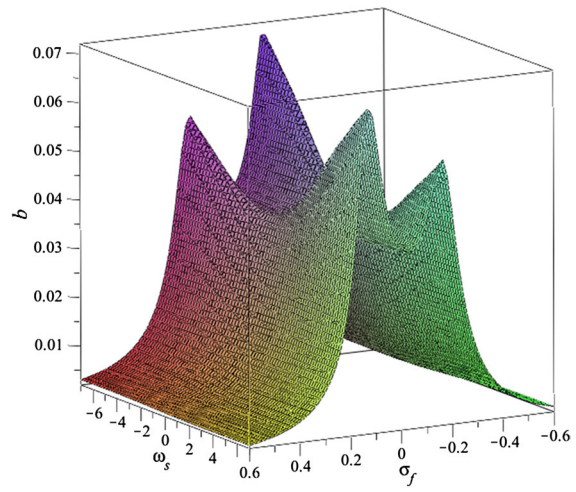

Fig. 11 NMPPF compensator amplitude versus excitation and lossy integrator frequencies

to have maximum vibration attenuation, the frequency of the second-order compensator has to be equal to the excitation frequency, regardless of the main system resonant frequency. It has been previously shown for linear systems with excitations at resonant frequency that the optimal value for the compensator frequency is the main system's frequency [21]. Figure 9 shows the controller amplitude in the suppression process. The minimum value on the line of $\sigma_r = \sigma_f$ occurs at $\sigma_r = \sigma_f = 0$. As the magnitude of the distance from origin on that line increases, the output amplitude increases too. The controller output on the rest of the (σ_r, σ_f) frequency plane could be considered as a function of $1/|\sigma_f - \sigma_r|$ in a rough estimation, where $|.|$ is the magnitude. As the difference increases, the controller output amplitude decreases.

Frequency of the first-order compensator (ω_s) is another parameter that impacts the closed-loop response of the system. Since the effect of the first-order compensator has to be studied over the excitation frequency domain, Fig. 10 is used to show the main system amplitude for the changes of both ω_s and σ_f. According to Fig. 10, variation of ω_s does not have a significant effect

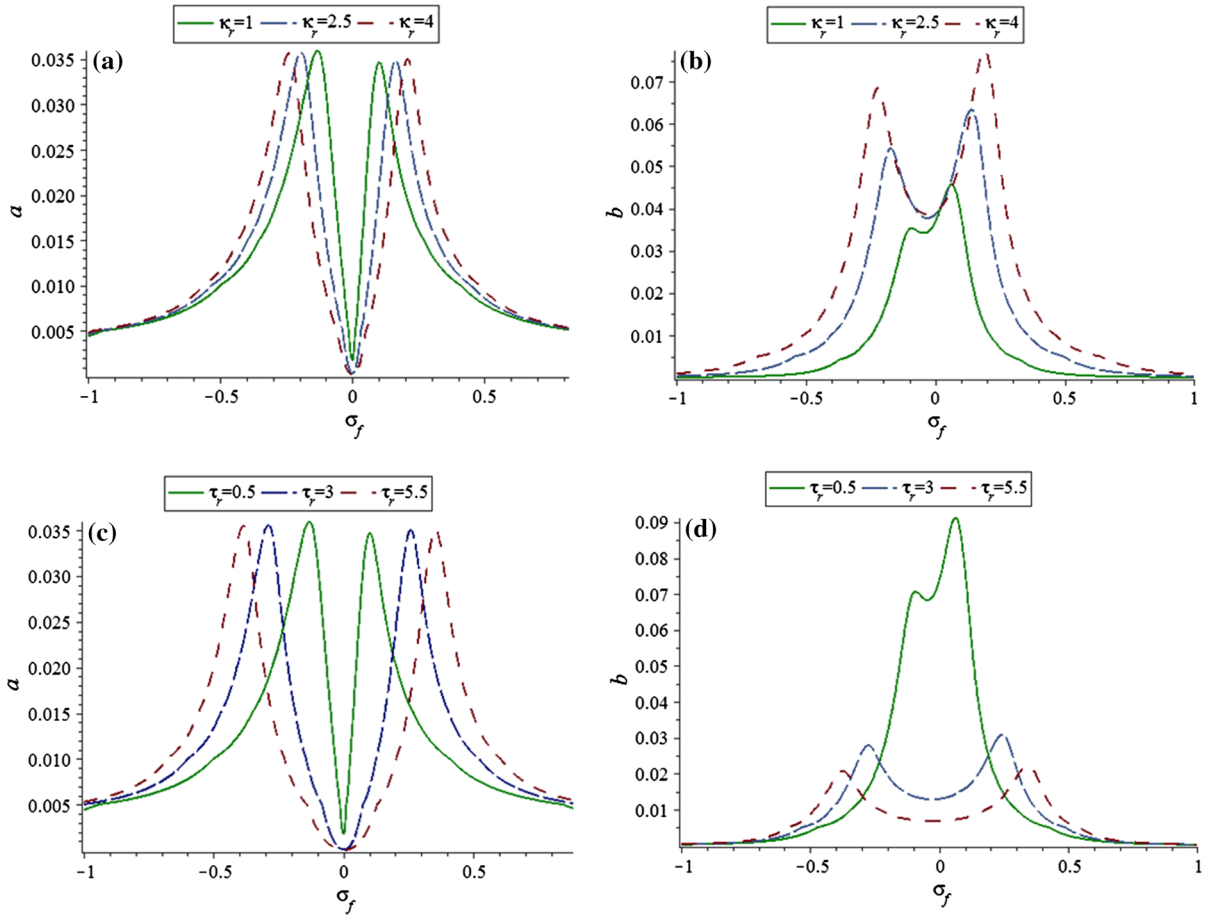

Fig. 12 Closed-loop system response to κ_r and τ_r variations

on the suppressed vibration amplitude at resonance (the line $\sigma_f = 0$). This is because the second-order compensator undertakes the larger share in resonant suppression compared to the first-order compensator. Nonetheless, it affects the amplitudes of the two peak values before and after the zero reference of the excitation detuning parameter. The minimum amplitude occurs at $\omega_s = 0$, where the lossy integrator becomes a simple integrator. Variation of ω_s also affects the second-order compensator amplitude b, as depicted in Fig. 11. As it was demonstrated before, the left-hand side peak in the compensator amplitude is maximum (see Fig. 7b). However, for negative values of ω_s, the right-hand side peak increases more as ω_s goes deeper in negative side.

Next, efficacy of the controller gains is studied. To this end, first, the gain values of the second-order compensator, κ_r and τ_r, are varied and the results are demonstrated in Fig. 12. According to Fig. 12a, increment of κ_r does not reduce the magnitude of the two peak values in the system response. Nonetheless, vibration amplitudes at resonance ($\sigma_f = 0$) are suppressed better as κ_r increases. According to Fig. 12b on the other hand, the second-order compensator amplitude increases proportional to κ_r. Increments in τ_r of the control law of Eq. (18) also result in better vibration amplitude suppression at exact resonant frequency (Fig. 12c). In addition, the two peak values occur at farther distances from the origin, as the graphs are widened in the frequency domain. Figure 12d shows that τ_r has inverse effect on the amplitude of the second-order amplitude.

Figure 13 shows the effect of changes in the first-order compensator gains, κ_s and τ_s. As it was discussed earlier that the second-order compensator suppresses the exact resonant amplitudes better, changes in κ_s and τ_s of the first-order compensator do not influence that

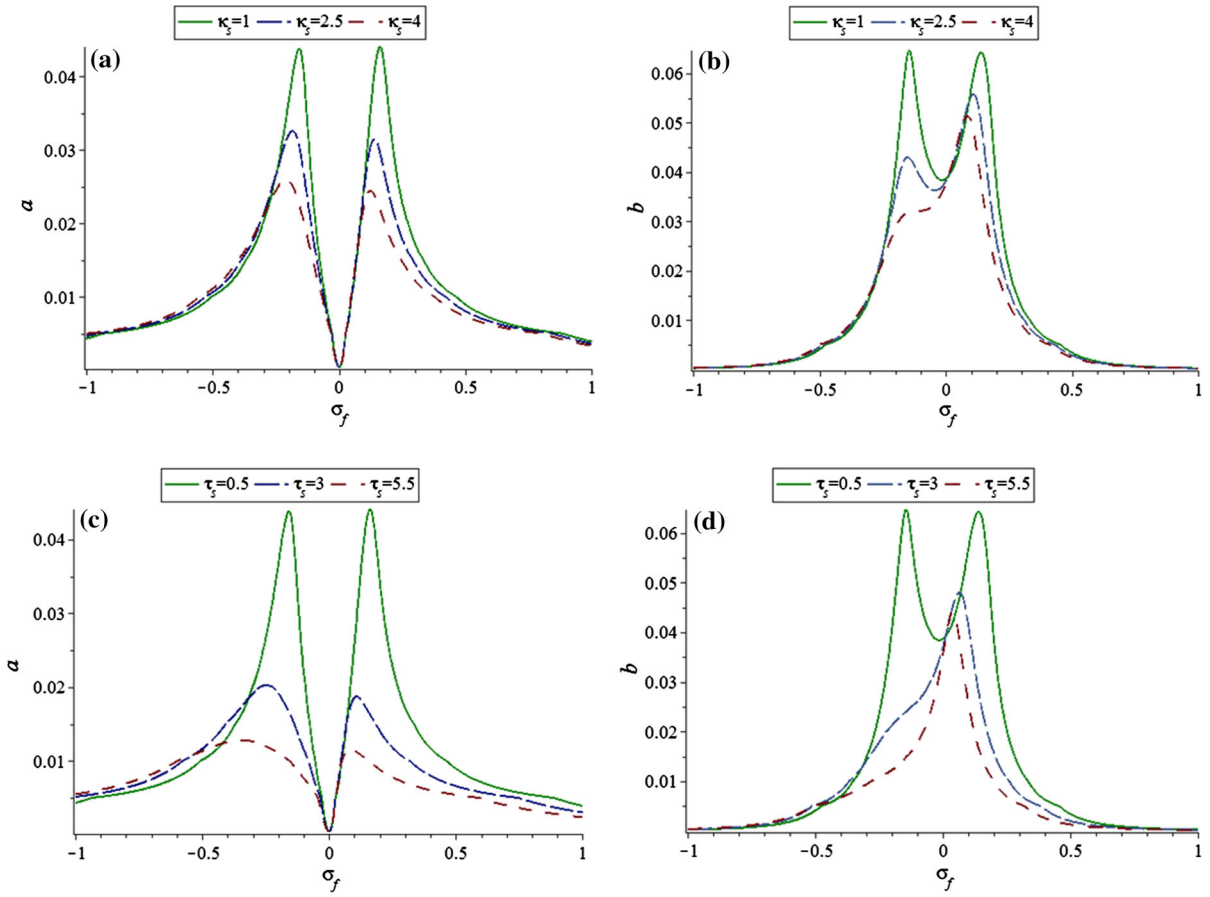

Fig. 13 Closed-loop system response to κ_s and τ_s variations

part of the solution in the graphs. $\sigma_f = 0$ is a fixed point in compensator amplitude graphs of Fig. 13b, d. This also implies that the changes in the amplitude of the first-order compensator do not affect the amplitude of the second-order compensator for $\sigma_f = 0$. However, higher gain values reduce the amplitude of the main system in peak values. Control output amplitudes also decrease as a result of main system amplitudes reduction.

Finally, the influence of the nonlinear term (δ) on the closed-loop system response is discussed. Existence of the nonlinear term makes the solution of the controller amplitude [Eq. (64)] system more complex. Figure 14 shows the NMPPF controlled system response for variations of δ. Implementation of the nonlinear term provides the opportunity to shift the minimum value of the frequency response that for $\delta = 0$ happens at $\sigma_f = 0$. Negative values of δ shifts the local minimum to left, and positive values shift it to right. The same shift in graphs happens for the compensator amplitude b.

6.4 Numerical and perturbation results comparison

In this section, numerical simulation results are presented in comparison with the approximation results. The excitation amplitude is considered as $f = 0.05$, and all gains are set equal to one. MATLAB® ode45 solver is implemented to solve the Eqs. (13), (16), and (17) numerically, to obtain the frequency response in the neighborhood frequencies of the fundamental mode. The results of the perturbation solution and the numerical results are shown in Fig. 15. According to the results, the approximation and numerical results are in good agreement with each other, as the result at exact resonant frequency ($\sigma_f = 0$) matches perfectly. The maximum errors occur in peak amplitudes.

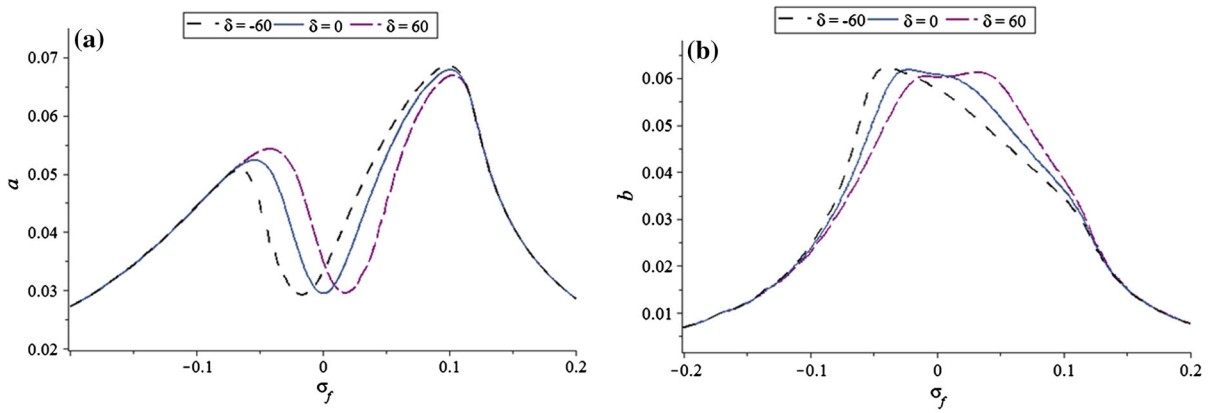

Fig. 14 Influence of nonlinear term (δ) on closed-loop system response, $\mu_r = 0.006$, and controller gains are set equal to 0.5

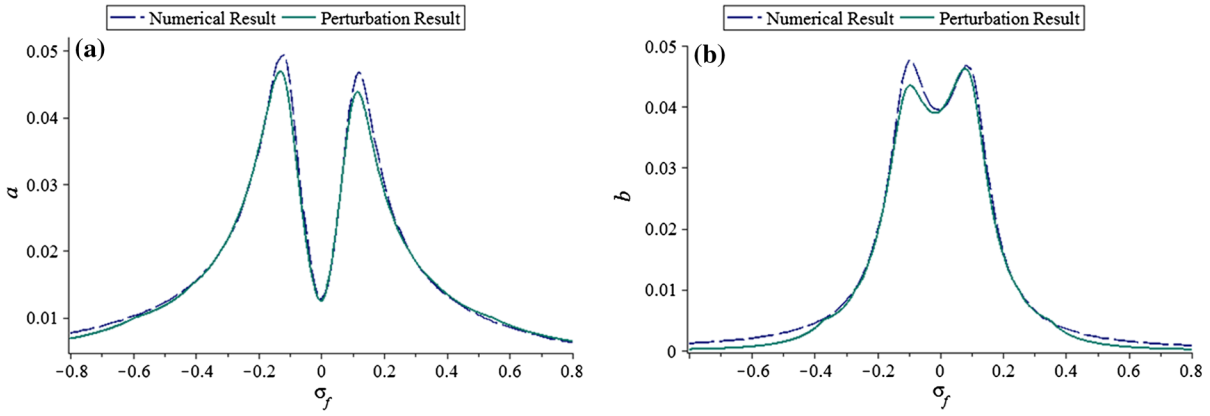

Fig. 15 Numerical and perturbation analysis results comparison

7 Conclusion

A new NMPPF controller was introduced in this paper for nonlinear vibration attenuation of the primary mode in presence of 1:1 internal resonance. The NMPPF controller has a cubic nonlinear term devised in a second-order resonant compensator accompanied by a lossy integrator. Method of Multiple Scales was implemented to obtain the closed-loop solution of the system. Stability analysis was performed on the system modulation equations. To show the controller efficiency, performance of the NMPPF and the conventional PPF controllers were compared. The NMPPF controller had a better suppression in the exact resonance, and also in overall frequency domain. Influences of the first- and second-order compensator frequencies were then discussed. Optimal value for the compensation frequency in nonlinear systems was extracted as a function of excitation frequency. In addition, the effects of the controller gains and the nonlinear term on the system response were presented and discussed. The nonlinear term provides the opportunity to shift the local minimum of the controlled frequency response graph to either side of the amplitude axes.

References

1. Marinca, V., Herisanu, N.: Nonlinear Dynamical Systems in Engineering: Some Approximate Approaches. Springer, New York (2012)
2. Nayfeh, A.H., Mook, D.T.: Nonlinear Oscillations, p. c1979. Wiley, New York (1979)
3. Mahmoodi, S.N., Jalili, N.: Non-linear vibrations and frequency response analysis of piezoelectrically driven microcantilevers. Int. J. Non-Linear Mech. **42**(4), 577–587 (2007)
4. Gao, J., Shen, Y.: Active control of geometrically nonlinear transient vibration of composite plates with piezoelectric actuators. J. Sound Vib. **264**(4), 911–928 (2003)

5. Mahmoodi, S.N., Jalili, N., Ahmadian, M.: Subharmonics analysis of nonlinear flexural vibrations of piezoelectrically actuated microcantilevers. Nonlinear Dyn. **59**(3), 397–409 (2010)
6. Shooshtari, A., Hoseini, S.M., Mahmoodi, S.N., Kalhori, H.: Analytical solution for nonlinear free vibrations of viscoelastic microcantilevers covered with a piezoelectric layer. Smart Mater. Struct. **21**(7), 075015 (2012)
7. Hosseini, S.M., Shooshtari, A., Kalhori, H., Mahmoodi, S.N.: Nonlinear-forced vibrations of piezoelectrically actuated viscoelastic cantilevers. Nonlinear Dyn. 1–13 (2014) . doi:10.1007/s11071-014-1461-7
8. Omidi, E., Korayem, A.H., Korayem, M.H.: Sensitivity analysis of nanoparticles pushing manipulation by AFM in a robust controlled process. Precis. Eng. **37**(3), 658–670 (2013)
9. Korayem, M.H., Omidi, E.: Robust controlled manipulation of nanoparticles using atomic force microscope. Micro Nano Lett. **7**(9), 927–931 (2012)
10. Alhazza, K.A., Daqaq, M.F., Nayfeh, A.H., Inman, D.J.: Non-linear vibrations of parametrically excited cantilever beams subjected to non-linear delayed-feedback control. Int. J. Non-Linear Mech. **43**(8), 801–812 (2008)
11. Jun, L., Xiaobin, L., Hongxing, H.: Active nonlinear saturation-based control for suppressing the free vibration of a self-excited plant. Commun. Nonlinear Sci. Numer. Simul. **15**(4), 1071–1079 (2010)
12. Warminski, J., Bochenski, M., Jarzyna, W., Filipek, P., Augustyniak, M.: Active suppression of nonlinear composite beam vibrations by selected control algorithms. Commun. Nonlinear Sci. Numer. Simul. **16**(5), 2237–2248 (2011)
13. Warminski, J., Cartmell, M.P., Mitura, A., Bochenski, M.: Active vibration control of a nonlinear beam with self- and external excitations. Shock Vib. **20**(6), 1033–1047 (2013)
14. Bouchard, M., Paillard, B.: Improved training of neural networks for the nonlinear active control of sound and vibration. IEEE Trans. Neural Netw. **10**(2), 391–401 (1999)
15. Ghandchi Tehrani, M., Wilmshurst, L., Elliott, S.J.: Receptance method for active vibration control of a nonlinear system. J. Sound Vib. **332**(19), 4440–4449 (2013)
16. Oueini, S.S., Nayfeh, A.H.: Single-mode control of a cantilever beam under principal parametric excitation. J. Sound Vib. **224**(1), 33–47 (1999)
17. Fanson, J.L., Caughey, T.K.: Positive position feedback control for large space structures. AIAA J. **28**(4), 717–724 (1990)
18. Jun, L.: Positive position feedback control for high-amplitude vibration of a flexible beam to a principal resonance excitation. Shock Vib. **17**(2), 187–203 (2010)
19. El-Ganaini, W., Saeed, N.A., Eissa, M.: Positive position feedback (PPF) controller for suppression of nonlinear system vibration. Nonlinear Dyn. **72**(3), 517–537 (2013)
20. Friswell, M.I., Inman, D.J., Rietz, R.W.: Active damping of thermally-induced vibrations. J. Intell. Mater. Syst. Struct. **8**(8), 678–685 (1997)
21. Mahmoodi, S.N., Ahmadian, M.: Active vibration control with modified positive position feedback. J. Dyn. Syst. Meas. Control **131**(4), 041002 (2009)
22. Omidi, E., Mahmoodi, S.N.: Active vibration control of resonant systems via multivariable modified positive position feedback. In: ASME Dynamic Systems and Control Conference, Anonymous AMSE, Stanford University, Palo Alto, CA (2013)
23. Omidi, E., McCarty, R., Mahmoodi, S.N.: Implementation of modified positive velocity feedback controller for active vibration control in smart structures. In: SPIE Smart Structures and Materials + Nondestructive Evaluation and Health Monitoring, Anonymous International Society for Optics and Photonics, pp. 90571N–90571N-11, San Diego, California, USA, (2014)
24. Mahmoodi, S.N., Craft, M.J., Southward, S.C., Ahmadian, M.: Active vibration control using optimized modified acceleration feedback with adaptive line enhancer for frequency tracking. J. Sound Vib. **330**(7), 1300–1311 (2011)
25. Meirovitch, L.: Principles and Techniques of Vibrations. Prentice Hall, Englewood Cliffs (1997)
26. Nayfeh, A.H.: Introduction to Perturbation Techniques. Wiley, New York (1981)
27. Hsieh, S., Shaw, S.W., Pierre, C.: Normal modes for large amplitude vibration of a cantilever beam. Int. J. Solids Struct. **31**(14), 1981–2014 (1994)
28. Mahmoodi, S.N., Khadem, S.E., Kokabi, M.: Non-linear free vibrations of Kelvin–Voigt visco-elastic beams. Int. J. Mech. Sci. **49**(6), 722–732 (2007)
29. Love, A.E.H.: A Treatise on the Mathematical Theory of Elasticity. Dover, New York (1944)
30. Kaliakin, V.N.: Introduction to Approximate Solution Techniques, Numerical Modeling, and Finite Element Methods. CRC Press, Boca Raton (2001)
31. Mahmoodi, S.N., Jalili, N., Daqaq, M.F.: Modeling nonlinear dynamics, and identification of a piezoelectrically actuated microcantilever sensor. IEEE Trans. Mechatron. **13**(1), 58–65 (2008)
32. Liao, X., Yu, P.: Absolute Stability of Nonlinear Control Systems, 2nd edn. Springer Science, New York (2008)